Combination of Phosphorous Flame Retardants and Aluminum Trihydrate in Multicomponent EPDM Composites

Benjamin Zirnstein, Dietmar Schulze, Bernhard Schartel
Bundesanstalt für Materialforschung und -prüfung (BAM), Unter den Eichen 87, 12205, Berlin, Germany

Ethylene propylene diene monomer (EPDM) rubbers with the flame retardants tris(2-ethylhexyl)phosphate, ammonium polyphosphate, polyaniline, and aluminum trihydroxide were prepared and analyzed in this study. The homogenous dispersion of the fillers in the rubber matrix was confirmed by scanning electron microscope. To investigate the interplay of the different flame retardants, the flame retardants were varied systematically. The comprehensive study sought combinations of flame retardants that allow high loadings of flame retardants without deterioration of the physical and mechanical properties of the EPDM rubber. The eight EPDM rubbers were investigated via thermogravimetric analysis and pyrolysis gas chromatography coupled with a mass spectrometer (Py-GC/MS) to investigate the potential synergistic effects. In the Py-GC/MS experiments, 27 pyrolysis products were identified. Furthermore, UL 94, limiting oxygen index, FMVSS 302, glow wire tests, and cone calorimeter tests were carried out. In the cone calorimeter test the EPDM rubbers R-1AP and R-1/2P achieved an increase in residue at flameout of 76% and a reduction in total heat evolved of about 35%. Furthermore, the compounds R-1AP and R-1/2P achieved a reduction in MAHRE to about 150 kW m^{-1}, a reduction of over 50% compared to the unprotected rubber R. POLYM. ENG. SCI., 60:267–280, 2020. © 2019 The Authors. *Polymer Engineering & Science* published by Wiley Periodicals, Inc. on behalf of Society of Plastics Engineers.

INTRODUCTION

Ethylene propylene diene monomer (EPDM) rubber is the most widely used synthetic rubber for nontire applications, such as automotive, construction, and electrical insulation. EPDM rubbers offer usage at low temperatures and have excellent weather and chemical resistance [1–3]. Like all carbon-based rubbers, EPDM burns easily, causing rapid fire spreading accompanied by the emission of high amount of dense smoke. To solve this problem, high amounts of flame retardants are usually applied to EPDM rubbers. Due to environmental and health issues in the past, halogen-free flame retardants are widely used. The most promising alternatives to flame retardants containing halogen are mineral flame retardants and phosphorous flame retardants [4, 5]. Aluminum trihydroxide (ATH) is widely used in elastomers in high tonnage because of its low cost [6]. The improved fire performance is achieved by fuel replacement in the condensed phase, and by cooling and fuel dilution in the gas phase. Furthermore, ATH forms a ceramic protective layer, which slows down the pyrolysis process [7–9]. ATH is applied in high loadings, usually 40%–70%, to achieve sufficient flame retardancy. Because of these high loadings, the mechanical properties of the rubber composites are often deteriorated [10, 11].

Consequently, the investigation of new solutions to improved flame retardancy with preserved mechanical properties is needed. Multicomponent flame retardant systems that exploit synergistic effects seem to be a promising solution [12–16]. The synergistic interplay of flame retardants depends on various parameters. The ratio of the flame retardants is key, to form reactive intermediates, resulting in synergistic effects [17]. If the synergistic interplay works efficiently, additional carbonaceous char is formed and influences the transport process between the flame and the pyrolysis zone [18, 19]. An alternative method to gain additional char is the combination of phosphorus flame retardants and nanofillers, such as layer silicates [20]. Whereas combinations of ammonium polyphosphate (APP) and aluminum hydroxide in ethylene-vinyl acetate achieved ceramifiable properties and improved flame retardancy due to increased residue [21]. Polystyrene with a combination of red phosphorus and magnesium hydroxide showed the formation of glassy metal phosphates causing better protection layer effects [22]. Nevertheless, studies had shown that using dispersed mineral fillers resulted in synergistic and antagonistic effects in the same matrix, depending on the combination of flame retardants [23, 24]. Furthermore, the synergistic effect of flame retardants containing aluminum and phosphorus depends on the specific surface area of the applied flame retardants [25]. The synergic effect may change with different particle sizes of the flame retardants [25]. Combinations of ATH and APP aim for the thermally stable P–Al–O surface coating to improve surface protection [26]. Previous studies described the synergistic interplay of aluminum hydroxide and aluminum hypophosphite with APP [27–29], and nanoparticles [1, 30, 31] in elastomers.

Former studies of our group investigated the impact of polyaniline (PANI), a potential char precursor, in EPDM rubbers with phosphorous flame retardants and in multicomponent flame retardant systems [27, 32]. This work is part of a series of three publications and focused on the interplay of the flame retardants containing aluminum and phosphorus in multicomponent flame retardant EPDM composites. This study investigated eight EPDM rubber compounds containing the phosphorous flame retardant APP and tris(2-ethylhexyl)phosphate (TOF), the polymeric synergist PANI and the mineral filler ATH, with systematic variation of the fillers. The eight EPDM rubbers were compounded and their mechanical as well as physical properties were investigated. Additionally, the impact of the fillers on ignitability and fire performance was determined. Furthermore, the influence of the fillers on decomposition products was quantified via pyrolysis gas

Correspondence to: B. Schartel; e-mail: bernhard.schartel@bam.de
DOI 10.1002/pen.25280
Published online in Wiley Online Library (wileyonlinelibrary.com).
© 2019 The Authors. *Polymer Engineering & Science* published by Wiley Periodicals, Inc. on behalf of Society of Plastics Engineers.
This is an open access article under the terms of the Creative Commons Attribution License, which permits use, distribution and reproduction in any medium, provided the original work is properly cited.

chromatography coupled with a mass spectrometer (Py-GC/MS) to investigate the interplay of the flame retardants.

EXPERIMENTAL

Materials

EPDM (Keltan 2,450, 48 and 4.1 wt% of ethylene and ethylidene norbornene, respectively), 2,2,4-trimethyl-1,2-dihydrochinolin (HS, Vulkanox HS/LG), zinc oxide (Zincoxyd aktiv), thiuram MS (Rhenocure Thiuram MS/C,) and cyclohexyl-2-benzothiazolsulfenamid (CZ, Vulkacit CZ/C) were supplied by Lanxess (Cologne, Germany). Carbon black (CB, N550) was obtained from Evonik Industries AG (Essen, Germany). Sulfur (99%) was supplied by Merck, Darmstadt, Germany. Stearic acid (stearic acid pure) was purchased from Baerlocher (Unterschleißheim, Germany). PANI was obtained from Chemos GmbH & Co. KG. (Altdorf, Germany) The flame retardant APP (ExolitAP 766 (TP)) was supplied by Clariant (Muttenz, Switzerland), TOF (tri-(2-ethylhexyl)-phosphat, Disflammoll TOF) was supplied by Rhein Chemie (Mannheim, Germany), and ATH (ATH, Apyral 200SM) was supplied by Nabaltec AG (Schwandorf, Germany). All chemicals were used as received, without predrying.

Preparation of the EPDM Compounds

EPDM and other ingredients were mixed in an internal mixer (HF Mixing Group) and afterwards compounded on a two-roll mill (HF Mixing Group). Table 1 lists all ingredients of the rubber compounds. The rolls had a temperature of 50°C, a speed of 8 rpm, and a friction of 1.1:1. The rubber compounds were mixed in two stages. In the first stage, EPDM was mixed with CB, HS, stearic acid, zinc oxide, and the flame retardants (APP, TOF, PANI, and ATH). In the second stage, the curatives, Thiuram MS, CZ, and sulfur, were added to the compound. The rubber compounds had a total mixing time of 10 min. The curing time at which 90% of the crosslinking took place (t_{90}) was detected with a dynamic moving die rheometer (D-MDR 300, Montech, Werkstoffprüfmaschinen, Buchen, Germany). Furthermore, the minimum (ML) and maximum (MH) torque were determined. The rubber composites were cured in a compression mold at a pressure of 300 bar and a temperature of 160°C. For the characterization of the rubber composites as well as for the mechanical and fire tests, sheets with varying thicknesses of 2, 3, and 6 mm were prepared.

Characterization

In accordance with ISO 37, five dumbbell samples of 2 mm thickness were used to perform the tensile tests. In accordance with ISO 527, Young's modulus, elongation at break, and yield stress were assessed with a stress–strain machine (Zwick/Roell Z010 instrument; Zwick, Germany), using three dumbbell samples of 2 mm thickness. In accordance with ISO 7619-1, the Shore A hardness was measured with three specimens with a thickness of 6 mm.

For the investigation of the surface of the rubbers, a scanning electron microscope (SEM, Zeiss EVO MA 10; Zeiss, Germany) with an acceleration voltage of 10 kV was used. The SEM micrographs were taken from the freeze-fractured gold-coated surfaces of EPDM rubber composites. The storage modulus (G') and dynamic loss factor (tan δ) as a function of temperature were determined with the MCR 501 Rheometer (Anton Paar, Germany) at 1 Hz and 0.1% strain amplitude. The measurements were carried out within a temperature range from −80°C to 70°C at a heating rate of 1°C min^{-1}.

A TPS 1500 (Hot Disk, Gothenburg, Sweden) was used to determine the thermal conductivity. According to ISO 22007-4, the Hot Disk sensor was placed between two samples with a thickness of 6 mm.

A Stanton Redcroft instrument in accordance with ISO 4589-2 (specimen size $112 \times 6.5 \times 3$ mm^3) was used to determine the limiting oxygen index (LOI). UL 94-V and UL 94-HB measurements were performed according to IEC 60695–11-10 (specimen size $125 \times 13 \times 3$ mm^3).

The cone calorimeter tests were carried out on specimens $100 \times 100 \times 3$ mm^3 in size with a cone calorimeter (FTT, East Grinstead, UK). The samples were positioned in a metal wire cage made of sheet steel with dimensions of 241×101 mm^2 (1 mm wire with 9 mm mesh size). The rubber in the metal wire cage was placed in the retainer frame, although the ISO 5660 standard prescribes the metal cage without retainer frame [33]. The samples were tested with a distance of 35 mm between sample and burner and with a heat flux of 50 kW m^{-2}, without changing the heat flux distribution at the surface [34]. All measurements were done in duplicate, a third measurement was only performed, when a deviation >10% in any measure occurred. The results were averaged.

Thermogravimetric analysis (TGA) was done on a TG 209 F1 Iris (NETZSCH Instruments, Selb, Germany). A total of 5 mg portions of cryomilled rubber were placed as powder in a ceramic

TABLE 1. Formulation of the produced EPDM composites.

	R	R-1	R-2	R-1/2	R-1P	R-1/2P	R-1AP	R-1/2AP
EPDM	100	100	100	100	100	100	100	100
APP		21		10.5	21	10.5	21	10.5
TOF			21	10.5		10.5		10.5
PANI					7.0	7.0	7.0	7.0
ATH							50	50
Antioxidant	0.5	0.5	0.5	0.5	0.5	0.5	0.5	0.5
Zinc oxide	5.0	5.0	5.0	5.0	5.0	5.0	5.0	5.0
Stearic acid	1.0	1.0	1.0	1.0	1.0	1.0	1.0	1.0
CB	30	30	30	30	30	30	30	30
CZ	1.0	1.0	1.0	1.0	1.0	1.0	1.0	1.0
Thiuram MS	2.0	2.0	2.0	2.0	2.0	2.0	2.0	2.0
Sulfur	1.5	1.5	1.5	1.5	1.5	1.5	1.5	1.5

 DOI 10.1002/pen

crucible and pyrolyzed under nitrogen with an applied heating rate of 10 K min^{-1}. All measurements were done in duplicate and the results were averaged.

The glow wire test was performed with respect to probable applications of the EPDM rubber compounds. Glow wire tests were carried out according to DIN EN 60695–2, with samples $10 \times 10 \times 3$ mm^3 in size. The glow wire flammability index (GWFI) is the highest temperature at which no flame occurred, or the visible flame extinguished within 30 s after the removal of the glowing wire. Additionally, the underlying paper has to be intact [35]. The glow wire ignition temperature (GWIT) is defined as the temperature which is 25°C higher than the maximum temperature of the tip of the glow wire that did not ignite the material during three subsequent tests [35].

The FMVSS 302 test was carried out according to DIN 75200. The tests were carried out on five samples with specimens $160 \times 10 \times 3$ mm^3 in size, according to the standard.

The Py-GC–MS measurements were carried out with a microfurnace double-shot pyrolyzer (PY3030iD; Frontier Laboratories, Japan), which was connected via a split−/splitless inlet port to a gas chromatograph (7890B; Agilent Technologies), combined with a mass selective detector (5977B; Agilent Technologies). The EI ionization energy of the MSD was 70 eV. The scan range was 15–550 amu. Then, 250 μg samples were introduced into the pyrolysis zone by gravimetric fall at 600°C and pyrolyzed in a helium atmosphere. An Ultra Alloy + −5 capillary column (l = 30 m, iD = 0.25 mm, film thickness = 0.25 μm) with a helium flow of 1 mL min^{-1} was used to separate the pyrolysis products. The column temperature was kept at 40°C for 2 min and afterwards increased at a rate of 10°C min^{-1} to 300°C, where it was held for 10 min. The temperature of the GC injector was 300°C. It was operated in a split mode of 1:300. The identification of the peak was done with the help of the NIST14 MS library.

RESULTS AND DISCUSSION

Curing Properties

The nonflame-retarded rubber R showed a scorch time of 2.88 min and reached t_{90} after 9.77 min, as shown in Fig. 1. After the maximum was reached, reversion in torque occurred, caused by cleaved sulfide crosslinks resulting from extended curing.

The phosphorous rubbers R-1, R-2, and R-1/2 exhibited lower torque than R. Table 2 shows that the addition of APP in R-1 decreased the crosslinking density, which resulted in lower torque. Furthermore, the adhesion of uncoated APP to EPDM was poor [36]. Therefore, the reinforcing effect was limited. TOF acted as plasticizer in R-2 and enhanced the slippage of the rubber polymer chains, which resulted in lower torque, as shown in Fig. 1. The compound R-1/2 showed both effects, reduced crosslinking and plasticizer effects. Additionally, R-1/2 showed a faster reversion in torque after the maximum was reached. The measurement was terminated after 5% reversion or 90 min were reached.

The addition of APP reduced the scorch time, whereas TOF showed an increased in scorch time, because of the plasticizing effect. Combination of APP and TOF in R-1/2 yielded a scorch time between R-1 and R-2. The rubbers containing PANI, R-1P, and R-1/2P, exhibited lower scorch time than R-1 and R-1/2, because amines accelerated the vulcanization, shortening the scorch time [37, 38].

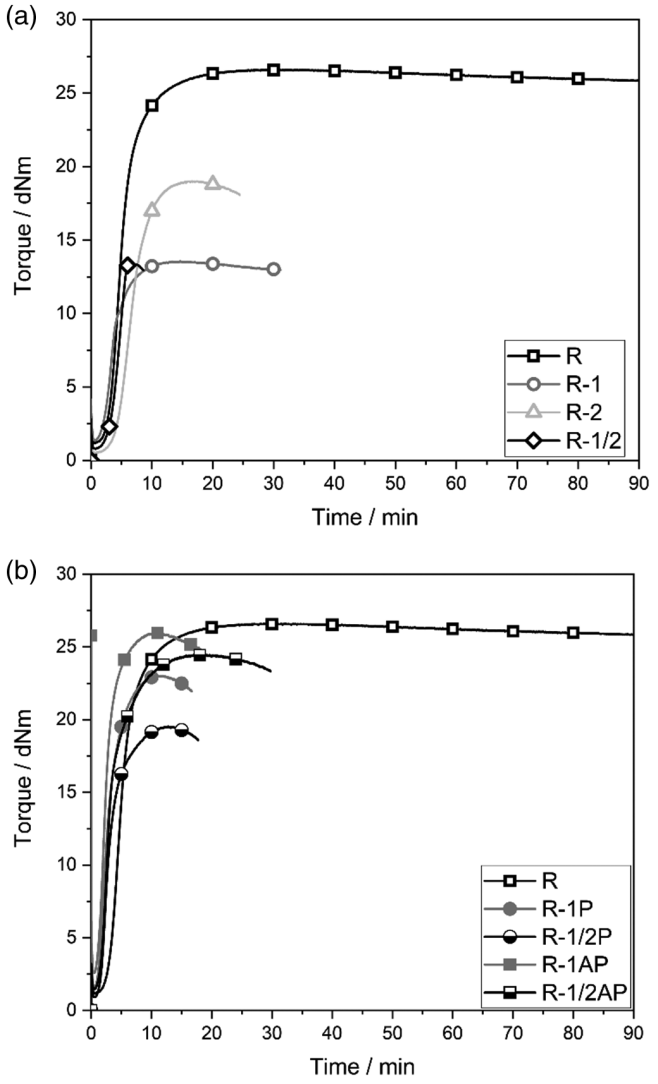

FIG. 1. Torque over time of the EPDM rubber compounds R, R-1, R-2, and R-1/2 (a) and the multicomponent flame retarded systems R-1P, R-1/2P, R-1AP, and R-1/2AP (b).

All rubbers except R-2 experienced a reduction in t_{90} due to the plasticizer effect, causing increased chain slippage. Only R-2 showed higher values for t_{90} than the unfilled rubber R. For the same reason, M_L is a measure of viscosity of the uncured rubber [39]. The rubbers containing TOF, R-2, R-1/2, and R-1/2P, exhibited lower minimum torque (M_L) compared to R. All the other flame retarded rubbers showed higher values for M_L, due to the reinforcing effect of the solid fillers APP, PANI, and ATH. Rubbers with higher filler loading and reinforcing fillers showed higher values for M_L [40, 41].

Table 2 presents the maximum torque (M_H), which is a measurement stock modulus [41]. R exhibited an M_H of 26.6 dNm. All rubber compounds exhibited a decrease in M_H as compared to the unfilled rubber R. Because APP had bad adhesion to the EPDM rubber matrix, the reinforcing effect was limited. TOF acted as a plasticizer and did not reinforce the rubber compound. PANI and ATH counteracted the effects from APP and TOF, leading to an increase in M_H.

M_H–M_L was used to assess the crosslink density of the EPDM rubbers qualitatively [40]. The results showed that the percentages

TABLE 2. Curing characteristics of the EPDM rubber compounds.

	R	R-1	R-2	R-1/2	R-1P	R-1/2P	R-1AP	R-1/2AP
Scorch time (±0.4)/min	2.88	1.88	3.57	2.62	1.14	1.44	1.21	1.33
t_{90} (±1.3)/min	9.77	7.11	10.14	5.58	6.07	6.70	5.04	8.18
M_H (±1.5)/dNm	26.6	13.6	19.0	13.6	23.0	19.5	25.9	24.5
M_L (±0.1)/dNm	1.17	1.35	0.51	0.79	1.60	0.92	2.57	1.44
M_H–M_L	25.4	12.3	18.5	12.8	21.4	18.6	23.4	23.0
Variation of the M_H–M_L /%	100	48	73	50	84	73	92	91

of the M_H–M_L values decreased with reduced network density, because of increased slippage between the polymer chains. All filled rubbers showed a decrease in crosslink density, which resulted from APP and TOF. The addition of PANI and ATH compensated for this effect in part. With the multicomponent flame retardant approach, the rubber compounds R-1AP and R-1/2AP preserved the curing behavior while simultaneously allowing high loadings of flame retardants.

Scanning Electron Microscopy

Figure 2 presents the SEM micrographs of the freeze-fractured surfaces of the EPDM rubbers. Figure 2a presents the unfilled rubber R. Because R had no additional filler, the surface was smooth. The addition of APP, seen in Fig. 2b, made the surface rougher, while the incorporation of TOF in R-2 led to a smoother surface, shown in Fig. 2c. The roughness of the surface of the compound R-1/2 was in between the roughness of the compounds R-1 and R-2. The addition of PANI yielded no change in roughness, as seen in the comparison of R-1P with R-1 and R-1/2P with R-1/2, whereas the rubber compounds containing ATH exhibited the roughest surface and highest protuberances. This effect is because ATH was applied in high loadings. ATH made the rubber compound stiffer and more brittle [42]. The particles, seen in Fig. 2e–h, are attributed to the flame retardants APP and ATH [43].

Mechanical Properties

Figure 3 and Table 3 present the results of the mechanical tests of all EPDM rubber compounds. The nonflame-retarded compound R showed an elongation at break of 330%. The rubbers R-1 and R-2 exhibited an increase in elongation at break compared to R. R-1/2, with a combination of APP and TOF exhibiting

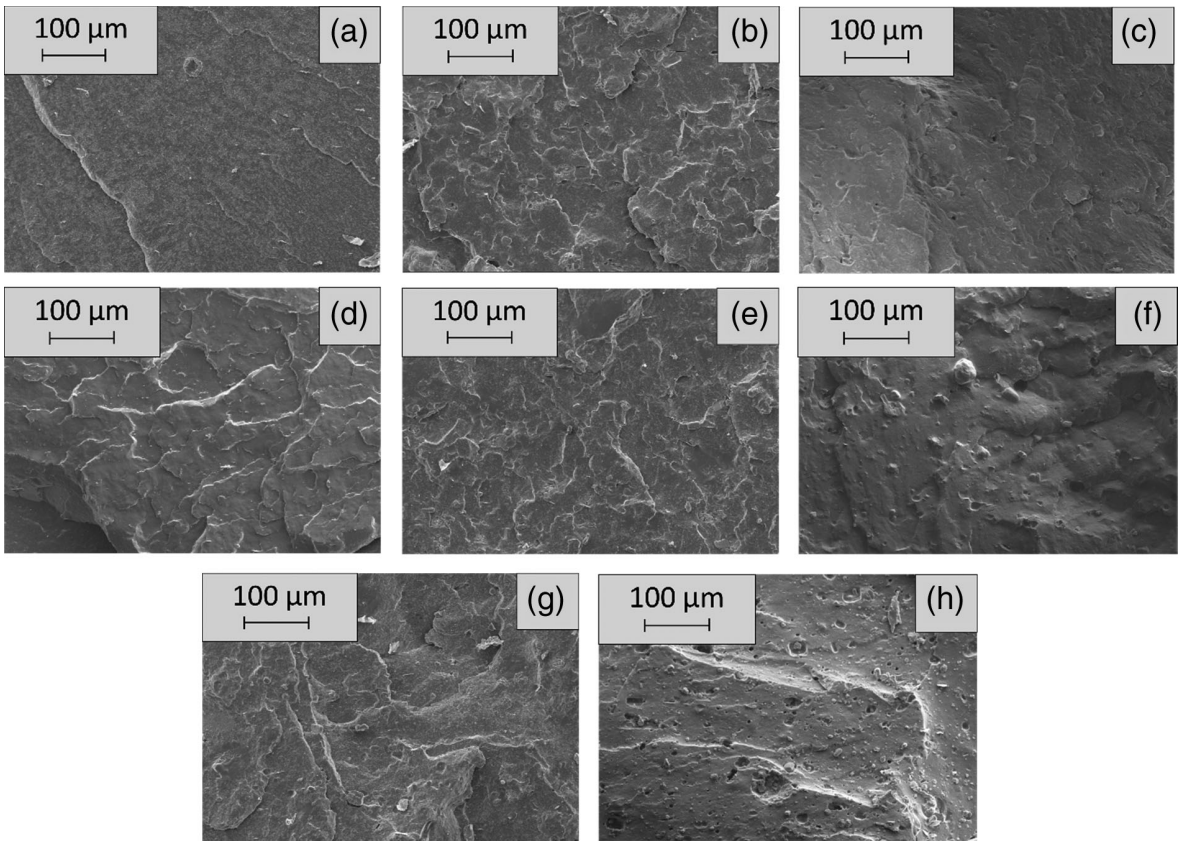

FIG. 2. SEM micrographs of the rubber composites R (a), R-1 (b), R-2 (c), R-1/2 (d), R-1P (e), R-1/2P (f), R-1AP (g), and R-1/2AP (h).

 DOI 10.1002/pen

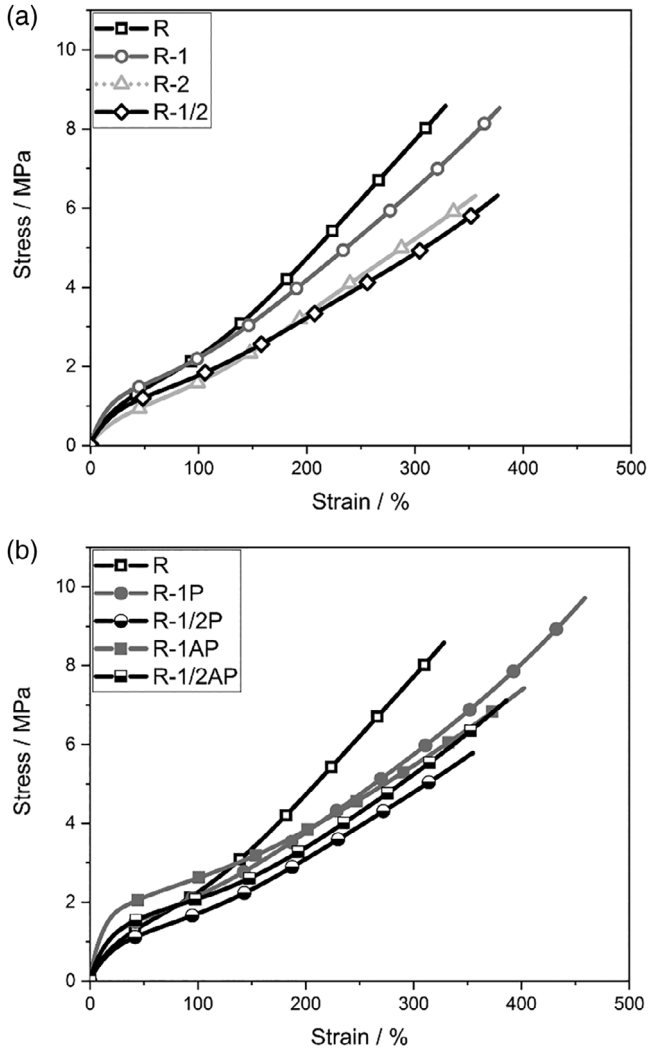

FIG. 3. Stress–strain curves of the EPDM rubbers R, R-1, R-2, and R-1/2 (a) and the multicomponent flame retarded rubbers R-1P, R-1/2P, R-1AP, and R-1/2AP (b).

an even higher increase than R-1 and R-2. The addition of PANI led to an 18% increase in elongation at break in R-1P, but a 10% decrease in R-1/2P, compared to the corresponding PANI-free compounds. Because the amount of PANI in R-1P and R-1/2P was similar, the TOF was responsible for the change in dispersion or filler–matrix interaction in R-1/2. The incorporation of ATH increased the elongation at break in R-1/2AP, but decreased the values in R-1AP compared to R-1/2P and R-1P. The reduction in elongation at break in R-1AP is explained by the high amounts of additional rigid fillers. The material became more brittle and broke earlier. Whereas the ATH in R-1/2AP had a positive effect, it compensated the plasticizing effect, reinforcing the composite, which resulted in higher elongation at break.

The nonflame-retarded compound R had a Young's modulus of 6.73 MPa (Table 3). The addition of APP in R-1 resulted in higher Young's modulus, due to the increased stress transfer from the rubber matrix to the filler. R-2 showed a lower Young's modulus than the unfilled compound R, because of the plasticizer effect of TOF. The Young's modulus of R-1/2 was in between the values of R-1 and R-2. In R-1/2, the reinforcing and the plasticizer effect canceled each other out, so that R-1/2 showed the same value as R. The addition of PANI in R-1P and R-1/2P left the Young's modulus unchanged compared to R-1 and R-1/2. The addition of ATH resulted in the highest Young's modulus, 28.5 MPa and 15.7 MPa. R-1AP had the highest value, because it contained the highest amount of rigid, reinforcing fillers. With higher amounts of fillers, interaggregate distances become smaller and the filler–filler interaction rises. In R-1/2AP, the reinforcing effect was limited by the plasticizer effect of TOF. Enhanced chain movement reduced the reinforcing effect. Nevertheless, R-1/2AP exhibited a 100% increase in Young's modulus compared to R.

The stress–strain curves of the EPDM compounds are presented in Fig. 3. The rubber compound R showed a tensile strength of 8.61 MPa and a stress at 100% elongation of 2.26 MPa, as shown in Table 3. R-1 exhibited values similar to R. The plasticizer TOF in R-2 led to lower values for tensile strength and stress at 100% compared to R. In general, all rubber compounds containing TOF, R-1/2, R-1/2P, and R-1/2AP, showed lower values for tensile strength and stress at 100% than the corresponding TOF-free samples R-1, R-1P, and R-1AP. In general, the results of elongation at break and tensile strength correspond well with each other. For elongation at break, the addition of PANI improved the mechanical properties in R-1P but resulted in lower values for tensile strength in R-1/2P. ATH in R-1AP led to a reduction in tensile strength compared to R-1P. The adhesion between filler and matrix determines the tensile strength and elongation at break. If the filler exhibits bad adhesion, failure originates in the interfacial region between the filler and rubber matrix [44]. The addition of ATH had a positive effect in R-1/2AP. The high amounts of rigid fillers compensated for the plasticizer effect of TOF, because of increased stress transfer from the matrix to the filler, and led to a tensile strength 20% higher than for R-1/2P.

Table 3 presents the hardness of all rubbers. The unfilled rubber R had a hardness of 66.9 Shore A. The addition of rigid fillers, APP, PANI, and ATH, increased the hardness. The incorporation of TOF led to a decrease in hardness, due to the plasticizer effect. The rubber compounds with the highest amount of fillers, R-1AP and R-1/2AP, showed the highest hardness values.

TABLE 3. Mechanical properties of the EPDM compounds.

	R	R-1	R-2	R-1/2	R-1P	R-1/2P	R-1AP	R-1/2AP
Elongation at break (±21)/%	330	378	348	388	446	355	422	373
Young's modulus (±0.5)/MPa	6.73	10.0	4.31	6.78	10.9	6.21	28.5	15.7
Tensile strength (±0.59)/MPa	8.61	8.51	6.22	6.34	9.12	5.81	7.86	6.90
Stress at 100% (±0.03)/MPa	2.26	2.16	1.61	1.75	2.01	1.74	2.60	2.10
Hardness (±0.6)/Shore A	66.9	68.3	55.7	59.3	69.0	62.3	77.1	70.5

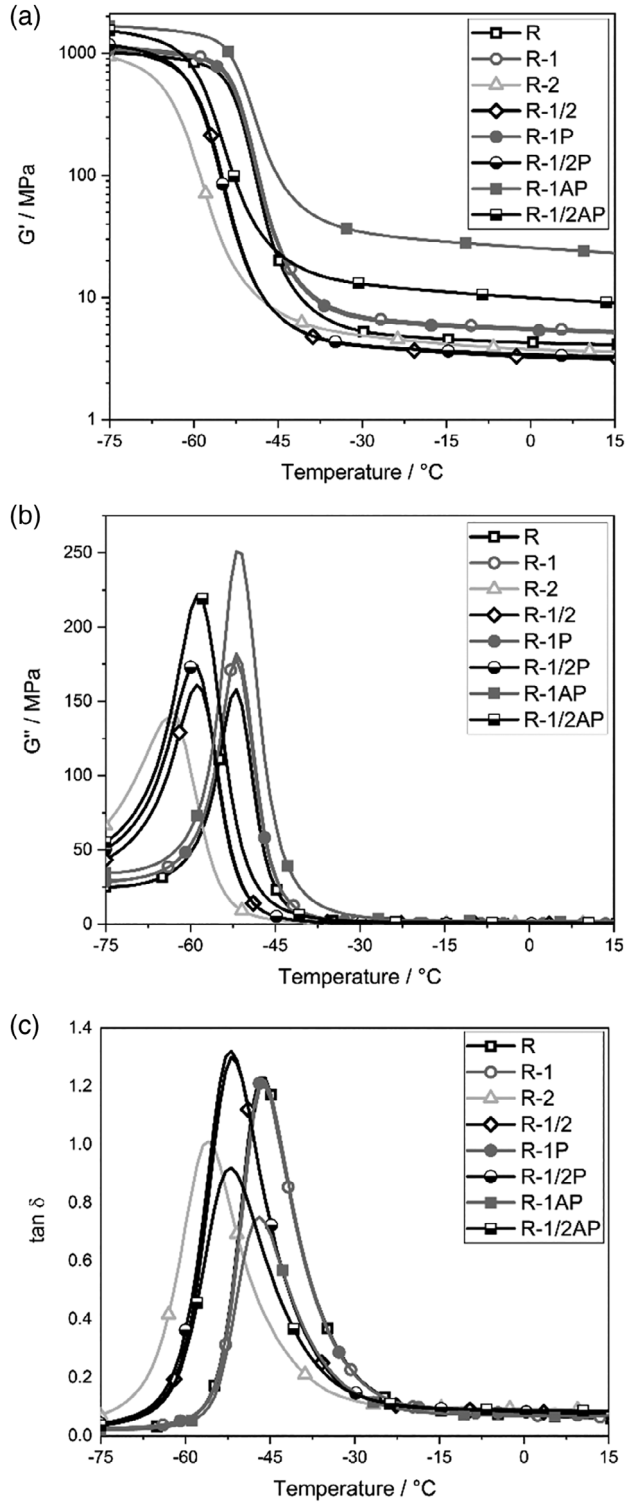

FIG. 4. Storage modulus (G') (a), loss modulus (G'') (b) and loss factor (tan δ) (c) as a function of temperature of all EPDM rubbers.

Dynamic Mechanical Properties

The results of the dynamic mechanical analysis (DMA) are presented in Fig. 4. The storage modulus (G') of the EPDM rubbers is shown in Fig. 4a. G' is related to the stiffness of the rubber. For this reason, the variation among the rubber compounds is more pronounced above the glass transition temperature (T_g), because the rubber itself is less stiff and the difference between the stiffness of the filler and the matrix becomes greater. The greatest impact on the overall stiffness came from the dynamic of immobilization of the rubber layers and stress transfer to the filler. The compounds R-1 and R-1P showed an increase in G' compared to R. This is due to the reinforcing effect of the rigid fillers APP and PANI. R-2 showed a different curve shape with an earlier decrease in G', indicating a lower T_g. This change was caused by TOF, acting as plasticizer, enhancing the chain movement that made the rubber less stiff. R-1 and R-1P exhibited a small increase in G' compared to R. R-1/2 and R-1/2P showed the same curve shape for G', with decreased T_g and a higher G' above T_g than in R. In general, the addition of PANI did not impact G'. The addition of ATH had the greatest impact on G', producing a strong increase above T_g. This corresponds well with the Young's modulus of the EPDM composites.

Figure 4b presents the loss modulus (G'') of the rubber compounds. The unfilled rubber R showed the second lowest maximum of all G''. Only R-2 exhibited lower values than R. Furthermore, the G'' maximum was shifted from −52°C to

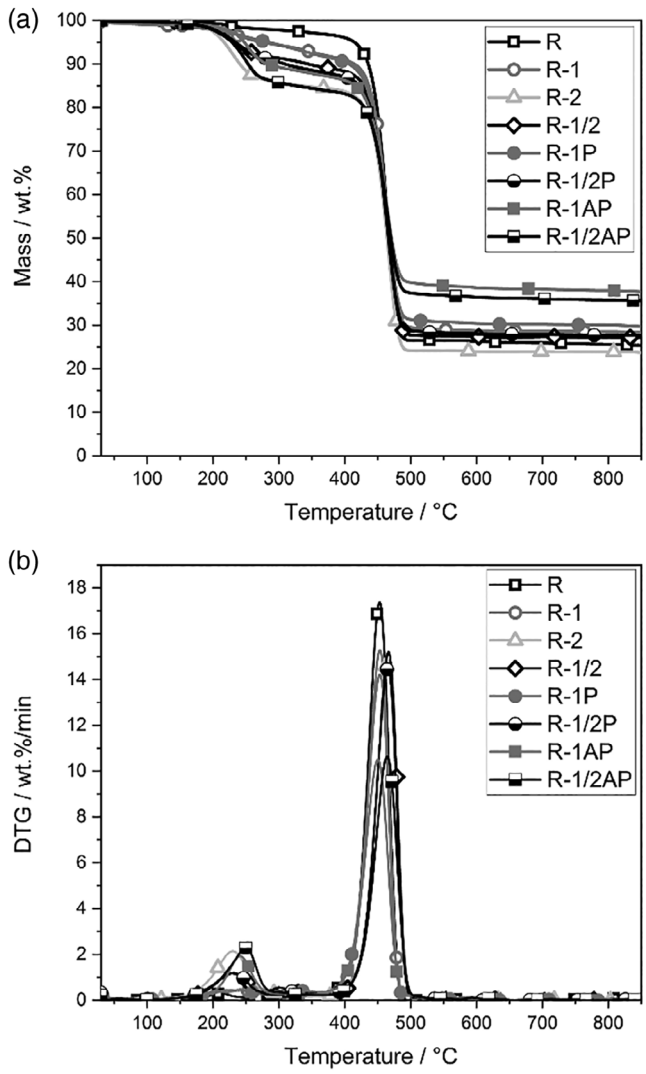

FIG. 5. Mass loss (a) and mass loss rate (b) of all EPDM compounds over temperature.

 DOI 10.1002/pen

TABLE 4. Results of the TGA of all EPDM rubber compounds. $T_{5\ wt\%}$, temperature at which 5 wt% of the mass was lost; T_{DTGmax} temperature of the maximum of the mass loss rate; residue of the rubber samples determined at 600°C.

	$T_{5\ wt\%}$ (±2)/°C	$T_{DTG(1)}$ (±2)/°C	Mass loss at $T_{DTG(1)}$ (±0.5)/wt%	$T_{DTG(max)}$ (±2)/°C	Residue (±1)/wt%
R	412	—	—	464	24.6
R-1	210	—	—	465	28.7
R-2	217	230	7.7	465	23.9
R-1/2	234	229	4.5	466	27.4
R-1P	215	—	—	465	30.4
R-1/2P	230	231	4.8	465	28.0
R-1AP	248	254	8.1	463	38.6
R-1/2AP	229	249	9.0	464	36.4

−63°C. These results correspond well with G'. The shift results from TOF acting as a plasticizer. The addition of APP and ATH resulted in a change in peak height, but caused no shift in temperature. The combination of APP and TOF in R-1/2 exhibited values for G'' like R. The reinforcing effect of APP and the plasticizing effect of TOF canceled each other out. R-1/2 experienced a shift of the peak of G'' from −52°C to −58°C. Investigating R-1P and R-1/2P, the addition of PANI in R-1/2P resulted in a higher G'', whereas the G'' of R-1P remained unchanged compared to the corresponding PANI-free samples R-1 and R-1/2. R-1, R-1P, and R-1/2P had the same height and same value of G'', meaning that similar amounts of energy were dissipated in heat. The compounds containing ATH showed the highest values of G''.

Figure 4c presents the loss factor (tan δ) of the EPDM compounds. The fillers in the rubber compounds had an evident effect on the energy dispersion. At lower temperatures, the values of tan δ were lower because the rubber itself was stiffer. The elastomers experienced higher viscosity, because hardly any movement of the rubber segments occurred, and the fillers had a limited effect on the energy dispersion [45]. The nonflame-retarded rubber R showed the peak of tan δ at −45°C, indicating that the α-transition of EPDM at T_g [46]. T_g was unchanged for R-1 and R-1P, but shifted to −55°C (−10°C) for R-2 and to −52°C (−7°C) for R-1/2, R1/2P, and R-1/2AP. The amount of TOF determined the change in T_g.

The addition of APP and PANI in R-1 and R-1P resulted in tan δ curves similar to those of the unfilled compound R. ATH in R-1AP reduced the peak height of tan δ. The reduction was caused by greater rubber–filler interaction, which restricted the motion of rubber chains. In R-1/2, APP led to higher values for the tan δ peak, indicating that more energy was dispersed as heat at lower temperatures. This corresponds well with the results from the mechanical tests and shows the poor filler–rubber interaction. The addition of PANI showed no impact on R-1/2 compared to R-1/2P. The rubber containing ATH exhibited the lowest values for tan δ, meaning that the rubber was more elastic, because the high amounts of ATH led to more rubber–filler interaction, restricting the movement of the rubber chains [45]. The amount of incorporated APP and ATH determined the values of tan δ. At temperatures above T_g the viscosity became lower, because the rubber molecules adjusted more rapidly and followed the dynamic strain, as the potential energy barriers were similar to the thermal energy [45].

Thermogravimetric Analysis

Figure 5, Table 4, and Table 5 present the results of the thermogravimetric analysis (TGA). The unfilled compound R had $T_{5\ wt\%}$ at 412°C. All other EPDM compounds exhibited $T_{5\ wt\%}$ at 210°C–250°C, because the flame retardants decomposed at lower temperature. All EPDM rubbers showed $T_{DTG(max)}$ at 465°C, the decomposition temperature of EPDM. The rubbers containing TOF, R-2, R-1/2, R-1/2P, and R-1/2AP, showed an additional first $T_{DTG(1)}$ at 230°C, the decomposition temperature of TOF. Because R-2 contained twice the amount of TOF compared to R-1/2P and R-1/2AP, the mass loss of R-2 was greater at $T_{DTG(1)}$. R-1/2AP had a greater mass loss at $T_{DTG(1)}$ than R-1/2P, because ATH had a decomposition temperature of 248°C and already started to decompose at $T_{DTG(1)}$. The addition of PANI led to an increase in residue in R-1P as compared with R-1, but not in R-1/2P as compared to R-1/2.

R showed residue of 24.6 wt%. The incorporation of APP in R-1 increased and the addition of TOF in R-2 decreased the formation of residue, compared to the unfilled compound R. The decreased amount of residue in R-2 occurred because TOF already decomposed at 230°C, went to the gas phase and showed

TABLE 5. The proportional contribution of the flame retardants on measured and calculated residues. The calculated residues are based on the previous TG results, with a margin of error of about ±1 wt%.

	Residue (±1)/wt%	Calc residue	Residue of EPDM	Residue of PANI	Residue of APP	Residue of TOF	Residue of ATH
R	24.6	—	24.6	0.0	0.0	0.0	0.0
R-1	28.7	27.3	21.4	0.0	5.9	0.0	0.0
R-2	23.9	21.7	21.4	0.0	0.0	0.3	0.0
R-1/2	27.4	24.5	21.4	0.0	3.0	0.1	0.0
R-1P	30.4	28.0	20.5	1.8	5.7	0.0	0.0
R-1/2P	28.0	25.2	20.5	1.8	2.8	0.1	0.0
R-1AP	38.6	36.5	15.8	1.4	4.4	0.0	14.9
R-1/2AP	36.4	34.4	15.8	1.4	2.2	0.1	14.9

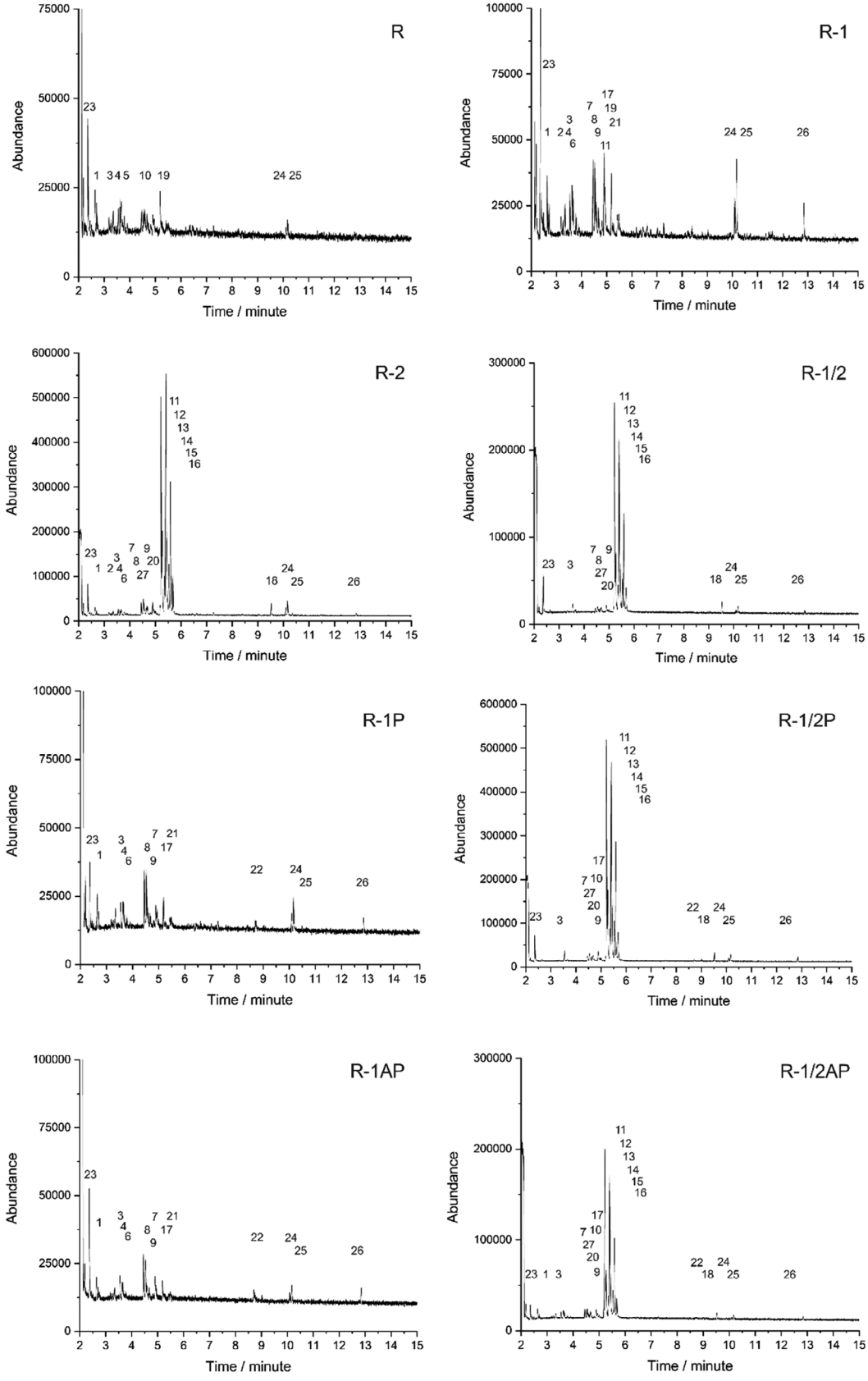

FIG. 6. Pyrograms of the rubber composites at 600°C.

 DOI 10.1002/pen

TABLE 6. Chemical compounds identified by Py-GC/MS of the EPDM rubber compounds.

Class	Compounds	Peak number	Retention time
Aliphatic	2-Methyl-1-pentene	1	2.702
	6-Methy-heptane	2	3.256
	Ethylidenecyclobutane	3	3.547
	3,3-Dimethylcyclobutanone	4	3.621
	Heptene	5	3.662
	1,2-Dimethyl-cyclopentane	6	3.712
	3-Methyl-1,3,5-hexatriene	7	4.457
	5,5-Dimethyl-1,3-cyclopentadiene	8	4.539
	4,4-Dimethylcyclohexadienone	9	4.542
	Cyclohexene-1-methanol	10	4.544
	3-Methylheptane	11	5.188
	3-Ethyl-3-hexene	12	5.270
	4-Octene (E)	13	5.360
	2-Octene (Z)	14	5.534
	3-Methyl-2-heptan	15	5.591
	2-Octene (E)	16	5.685
	2,2-Dimethylcyclopentanone	17	5.188
Aromatic	2-*tert*-Butyl-3,4,5,6-tetrahydropyridine	18	9.518
	Toluene	19	4.895
	Hydrazinecarboxylic acid	20	4.940
	Propoxymethylbenzene	21	4.936
	Aniline	22	8.725
Sulfurous	Carbon disulfide	23	2.361
	2,4,6-Triphenyl-1,3,5,trithiane	24	10.100
	2-Mercaptobenzylalcolhol	25	10.171
	Isothiocyanatocyclohexane	26	12.849
Phosphorous	Bis(6-methylheptyl)-dihydrogen-diphosphate	27	4.643

no contribution to the residue formation, as shown in Table 5. The combination with TOF and APP in R-1/2 led to an increase in residue compared to R. The increased residue of the rubber compounds containing APP and ATH results mainly from the residue that was formed after the decomposition of APP and ATH, namely polyphosphate and aluminum oxide, displayed in Table 5. Because TOF decomposed almost completely, the rubbers containing TOF exhibited less residue. Table 5 presents the calculated and the measured residues. The measured residues are 1.4%–2.9%, higher than the calculated residues. That means that the residue of each rubber compound is the total of all residues formed from each filler. Therefore, a limited additional char forming process was detected.

Pyrolysis Gas Chromatography Coupled with a Mass Spectrometer

The Py-GC–MS measurements investigated the pyrolysis products from the rubber compounds evolving at 600°C (Fig. 6). A total of 27 compounds were identified and are listed Table 6. Nine peaks were identified in the pyrogram of the nonflame-retarded rubber R. The aliphatic compounds 2-methyl-pentene (1), ethylidenecyclobutane (3), 3,3-dimethylcyclobutanone (4), heptane (5), cyclohexene-1-methanol (10), 2,2-dimethylcyclopentanone (17) were found in the pyrogram of R. Ethylidenecyclobutane (3) was formed by decomposition of the unsaturated backbone of EPDM, which is composed ethylene–propylene units. Toluene (19) resulted from the decomposition and rearrangement of the volatile products of the ENB unit of the EPDM rubber polymer [47]. Carbon disulfide (23), 2,4,6-triphenyl-1,3,5,trithiane (24), and 2-mercaptobenzylalcolhol (25) were the sulfurous molecules. Sulfur was used for vulcanization. An alternative sulfur source for isothiocyanatocyclohexane (32) is the applied vulcanization accelerator *N*-cyclohexyl-2-benzothiazolesulfenamide. In fact, all rubbers contained the sulfurous compounds carbon disulfide (23), 2,4,6-triphenyl-1,3,5,trithiane (24), and 2-mercaptobenzylalcolhol (25).

The pyrogram of R-1 showed a greater number of peaks. The incorporation of APP led to more aliphatic compounds in the pyrogram, as compared to the pyrogram of the unfilled EPDM rubber R. The additional compounds 2-ethyl-1-pentene (1), 6-methy-heptane (2), ethylidenecyclobutane (3), 3,3-dimethylcyclobutanone

TABLE 7. LOI, glow wire, and UL 94 results for the EPDM rubbers.

	R	R-1	R-2	R-1/2	R-1P	R-1/2P	R-1AP	R-1/2AP
LOI (±0.2)/vol%	20.6	25.0	23.6	22.2	24.0	23.0	26.6	25.0
GWIT (±25)/°C	700	700	750	750	700	700	825	850
GWFI (±25)/°C	775	900	825	800	960	775	960	960
UL 94	HB	HB	HB	HB	HB	HB	HB	HB
UL 94/mm × min^{-1}	18.2	0.5	22.3	22.8	3.9	7.7	0	2.5
FMVSS 302/mm × min^{-1}	27.5	0	20.2	11.0	0	16.7	0	0

(4), 1,2-dimethyl-cyclopentane (6), 3-methyl-1,3,5-hexatriene (7), 5,5-dimethyl-1,3-cyclopentadiene (8), 4,4-dimethylcyclohexadienone (9), and 3-methylheptane (11) were identified. The additional aromatic compound propoxymethylbenzene (21), like toluene (19), was formed from the ENB unit, by C—C bond cleavage, creating biradical intermediates, followed by rearrangement. The decomposition of APP released high amounts of ammonia and increased the formation of isothiocyanatocyclohexane (26).

The pyrogram of R-2 showed a set of signals similar to R-1. The additional signals 3-Methylheptane (11), 3-ethyl-3-hexene (12), 4-octene (E) (13), 2-octene (Z) (14), 3-methyl-2-heptan (15), and 2-octene (E) (16), and bis(6-methylheptyl)-dihydrogen diphosphate (27) were pyrolysis products of the flame retardant TOF. The aromatic compound 2-*tert*-butyl-3,-4,5,6-tetrahydropyridine (18) was detected only in the rubber compounds containing TOF, R-2, R-1/2, R-1/2P, and R-1/2AP. The pyrogram of the rubber R-1/2 with a mixture of APP and TOF showed signals similar to the compound R-2. Therefore, no interplay of APP and TOF was detected. In the pyrograms of the rubbers containing PANI, R-1P, R-1AP, R-1/2P, and R-1/2AP, two additional signals of 2,2-dimethylcyclopentanone (17) and aniline (22) were identified.

In general, the pyrograms of the flame retardant rubbers showed a greater number of decomposition products. However, all of the additional products resulted from the decomposition of the flame retardant. The pyrograms did not reveal any new decomposition products, which would suggest interplay between the various flame retardants.

FLAMMABILITY

The flammability of the EPDM compounds was evaluated with the UL 94, LOI, glow wire, and FMVSS 302 tests. The results are presented in Table 7. All flame retardant rubbers exhibited higher LOI values than the nonflame-retarded rubber R. The addition of APP led to an increase to 25.0 vol%, and TOF to 23.6 vol%. The combination of APP and TOF in R-1/2 showed values of 22.2 vol %. The combination of APP and TOF performed worse than either flame retardant individually, indicating an antagonistic effect. The addition of PANI led to no improvement, but the incorporation of ATH resulted in an increase in LOI [48].

Table 7 presents the results of the glow wire tests, the GWIT and the GWFI. The unfilled rubber compound R had a GWIT of 700°C and GWFI of 775°C. R-1, R-1P, and R-1/2P exhibited similar values for GWIT. The addition of TOF led to an increase in GWIT in R-2 and R-1/2 to 750°C. The rubbers containing ATH, R-1AP, and R-1/2AP, showed the highest GWIT values. The compounds containing TOF, R-2, R-1/2, and R-1/2AP, outperformed the corresponding TOF-free compounds R-1 and R-1AP. This effect is explained by the early decomposition of TOF, which released phosphorous species to the gas phase and delayed ignition. R-1 showed a GWFI value of 900°C, and R-2825°C. With a GWFI of 800°C, the combination of APP and TOF in R-1/2 showed lower values for GWFI than R-1 or R-2, indicating an antagonistic interplay of APP and TOF. In terms of GWFI, APP was more effective than TOF, as shown by the comparison of R-1 with R-2 as well as R-1P with R-1/2P. The EPDM rubbers R-1, R-1AP, and R-1/2AP achieved the highest rating with 960°C.

As shown in Table 7, all rubbers received HB classification in the UL 94 test. The burning speed of the rubbers in the UL 94 test and FMVSS were measured, and both values were in good agreement. The addition of APP reduced the burning speed significantly, and in combination with PANI and ATH in R-1AP, the rubber even experienced self-extinguishment in the horizontal UL 94 test. The incorporation of TOF led to an increase in burning speed. In fact, R-2 and R-1/2 showed higher burning speed than the unfilled EPDM rubber. The increase was caused by the plasticizer effect of TOF, as the softer rubbers burned more easily. Increased crosslinking provides additional covalent bonds, which must be broken before stepwise decomposition of the chain occurs in pyrolysis. Lower degrees of crosslinking decrease the thermal decomposition by increasing the distance between the polymeric chains. Furthermore, a greater degree of crosslinking promotes the formation of char [49]. In contrast to the UL 94 test, all flame retarded rubber samples showed reduced burning speed in the FMVSS 302 test compared to R. The rubber compounds with good results in the UL 94 test, R-1, R-1P, R-1AP, and R-1/2AP, experienced self-extinguishment in the FMVSS 302 test.

FIRE BEHAVIOR

Table 8 summarizes the results from the cone calorimeter tests. The ignitability and burning behavior of the EDPM rubbers in a well-ventilated developing fire scenario were tested. The unfilled rubber R showed ignition after 50 s. All flame retarded rubbers ignited earlier than unprotected rubbers. Due to earlier decomposition of the flame retardants, many flame retarded systems ignite earlier than nonflame-retarded systems [50].

Figure 7(a) presents the HHR curves of the EPDM compounds. The rubber compounds showed the typical curve shape for thermally thick charring materials with poor protective properties [51]. After ignition, the first peak occurred, the peak of heat release rate (PHHR), followed by a second lower and broader peak. In general, the addition of APP and ATH resulted in a reduction of HRR compared to the unfilled EPDM rubber R, whereas R-2, with TOF, showed a HRR curve similar to R. The combinations of APP and TOF in R-1/2, R-1/2P, and R-1/2AP experienced a reduction of HHR, but less than the TOF-free compounds R-1, R-1P, and R-1AP. APP formed a residue layer which limited the release of the volatiles and protective layer, acting as a heat shield. This mode of action is well known for phosphorous flame retardants [52–54]. In contrast, the TOF did not form a protective layer. TOF decomposed early and was released into the gas phase, but showed no significant gas phase activity and therefore did not reduce the HRR. The second peak in the HHR curve resulted from the thermal feedback when the pyrolysis front reached the back of the specimen [55]. Additionally, the cracking of the protective layer is a reasonable explanation for the second peak [51].

The nonflame-retarded rubber R showed the highest values for PHRR (598 kW m^{-2}). The addition of APP reduced the PHHR R-1 by 33% (399 kW m^{-2}). The flame retardant TOF had no impact on PHHR (582 kW m^{-2}). The addition of APP in R-1 showed a reduction of −200 kW m^{-2} compared to R. In combination with TOF in R-1/2 (502 kW m^{-2}), this reduction was halved to −100 kW m^{-2}. Because half the amount of APP was used in R-1/2, the reduction was halved as well. The incorporation of PANI left the PHRR unchanged, whereas the addition of ATH reduced the PHHR by about 50% compared to R. In general, the

TABLE 8. Cone calorimeter results of EPDM rubber composites with an irradiance of 50 kW m^{-2}.

	R	R-1	R-2	R-1/2	R-1P	R-1/2P	R-1AP	R-1/2AP
t_{ig} (±2)/s	50	43	40	37	37	36	48	45
PHRR (±5)/ kW m^{-2}	598	399	582	502	440	535	294	334
Flameout (±5)/s	315	366	354	381	408	381	546	426
Residue (±1)/wt%	30	40	25	30	39	35	50	53
THE (±4)/MJ m^{-2}	93	78	99	93	76	85	65	63
EHC (±0.5)/ MJ kg^{-1}	41.6	35.6	37.6	38.7	33.7	36.0	31.9	32.9
FIGRA (±0.2)/ kW m^{-2} s^{-1}	7.1	5.7	7.2	6.9	5.7	7.1	3.9	4.4
MARHE (±5)/ kW m^{-2}	314	231	347	283	231	289	142	167

combinations of APP and TOF were not as effective as APP alone.

Figure 7b presents the THR curves of the EPDM compounds. In general, all flame retarded rubbers showed a lower THR, except R-2. The compounds R and R-2 showed similar THR curves. The addition of APP in R-1 reduced the THR compared to R, as shown in Table 8. The compound R-1/2 exhibited a less pronounced reduction, because less APP was used. The rubbers containing PANI, R-1P, and R-1/2P, showed lower values for THR than R-1 and R-1/2. This minor improvement effect was caused by fuel replacement. PANI had a lower fire load than the EPDM polymer. Because ATH was applied in high loadings, the addition of ATH led to the most prominent reduction of THR. ATH acted through fuel dilution and fuel replacement. The total heat evolved (THE), which is the THR at flameout, is a measurement of the fire load of a material in the cone calorimeter fire scenario [51]. Table 8 presents the THE values of the rubber compounds.

The unprotected rubber R showed a THE value of 93 MJ m^{-2}. R-1 exhibited a reduction of 16% compared to R. TOF had no positive effect and R-2 had an even higher THE value than the unprotected R. The combination in R-1/2 performed like R. The negative impact of TOF is also a result of the plasticizer effect. PANI had a positive effect on THE and showed a greater reduction in R-1/2P (−9%) than in R-1P (−3%), as compared to R-1 and R-1/2, respectively. The addition of ATH led to a further

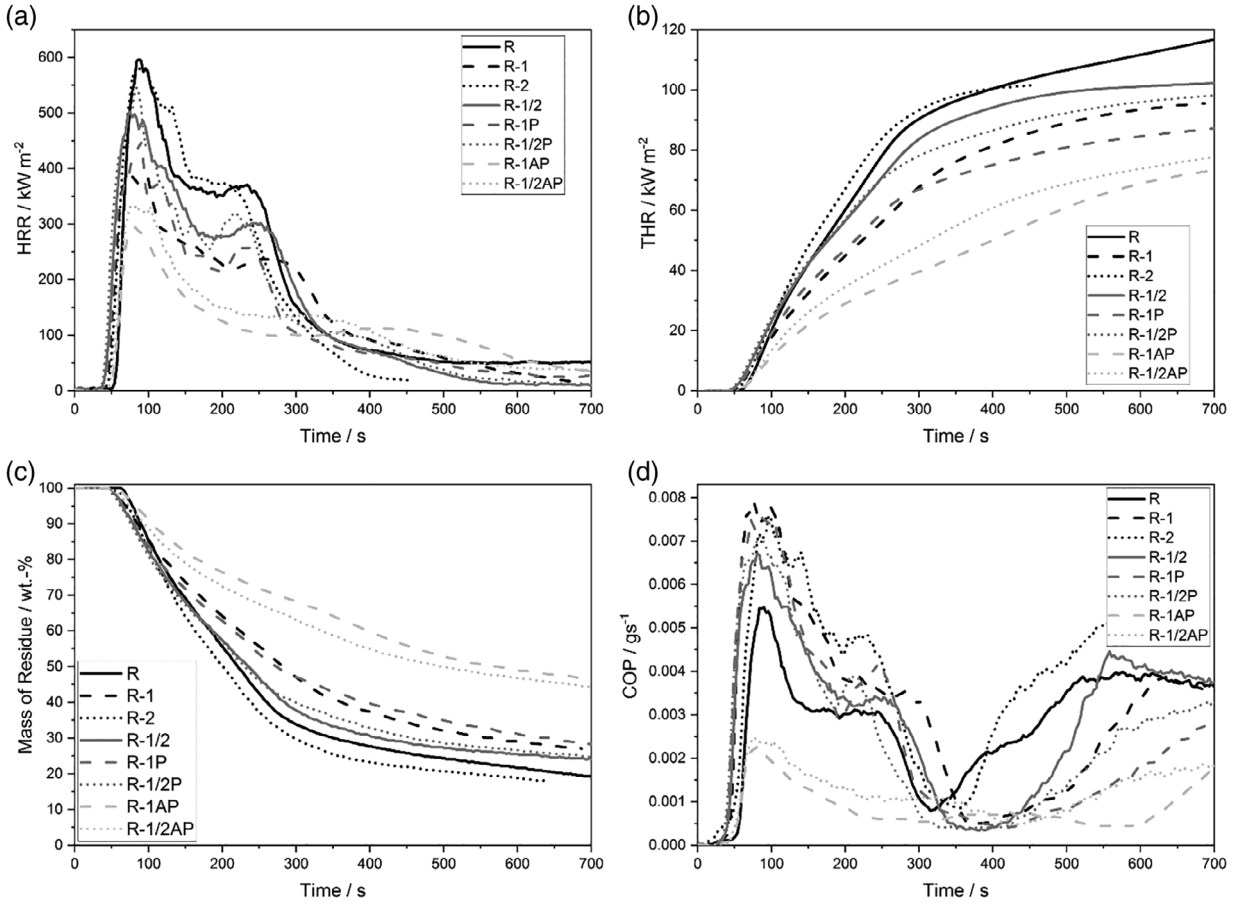

FIG. 7. Heat release rate (HRR) curves (a), total heat release rate (THR) curves (b), mass of residue, (c) and the COP (d) over time of the EPDM rubber compounds.

reduction in THE. The multicomponent rubbers R-1AP and R-1/2AP showed the lowest values for THE and achieved a reduction of up to 33% compared to the unprotected compound R.

Figure 7c presents the formation of residue of the EPDM rubbers. The residue of the unprotected rubber R mainly results from the filler CB. Under anaerobic conditions, the carbon fillers were thermally stable and therefore did not decompose during the pyrolysis phase. The anaerobic decomposition occurred while the rubber was burning with a stable flame [56]. The amount of residue left at the end of combustion is a parameter to quantify the condensed phase activity of flame retardants. Additionally, the formation of residue at flameout is strongly related to the fire load of a material. The addition of APP and ATH increased the amount of residue. Compared to the unfilled rubber R, R-1 showed an increase in residue of 10 wt%, whereas the flame retardant TOF led to a reduced (−5 wt%) residue formation to 25 wt%. In the combination R-1/2, these two effects, the positive effect of APP and negative impact of TOF, canceled each other out, so that R-1/2 exhibited the same amount of residue as the unfilled rubber R. One reason for the lower amount of residue in R-2 is that TOF decomposed almost completely and did not contribute to the residue. These results correspond well with the GA measurements. In R-1P the addition of PANI did not change the residue as compared to R-1. However, in combination with APP and TOF in R-1/2, PANI led to an increase in residue (+10 wt%) compared to R-1/2. PANI overcompensated the impact of TOF. The rubber R-1/2 had a PANI loading of 5%, and a former study showed that PANI left about 44% residue [27]. Therefore, the combination of PANI and TOF showed synergist effects in fuel fixation. The addition of ATH exhibited the greatest impact on the formed residue, because ATH was applied in high loadings. Compared to the corresponding ATH-free rubbers, the additional formed residue is mainly inorganic ceramic material which was formed from ATH. Nevertheless, the compound R-1/2AP exhibited a greater improvement (+18 wt%) than R-1AP (+11 wt%), compared to R-1/2P and R-1P, respectively. These results correspond well with the THE values.

The effective heat of combustion (EHC) is THE divided by the mass loss and is a measurement for the gas activity of the flame retardants [53]. The unfilled rubber R showed the highest values with 41.6 MJ kg^{-1}. Comparing the two rubbers R-1 and R-2, it was concluded that APP was more active in the gas phase than TOF. This means that TOF neither contributed to the formation of residue nor showed any significant gas activity. This explained the poor performance of R-2 in the fire test. The combination of APP and TOF in R-1/2 showed even worse gas phase activity, indicating an antagonistic interplay of APP and TOF. PANI led to improved gas activity in both R-1P and R-1/2P. Either PANI increased the gas activity of the phosphorous flame retardants, or it contributed nitrogen to the gas phase, which caused flame dilution. The rubbers containing ATH showed the best performance, with EHC values of about 32 MJ kg^{-1}. The increased gas phase activity was caused by flame dilution, due to the release of water from ATH.

After flameout, thermal-oxidative decomposition, called afterglow, took place [56]. Figure 7d presents the carbon monoxide production (COP) curves of the EPDM rubbers. During the burning phase, where pyrolysis occurred, the shape of the COP curves was like the shape of the HHR curves. The curves showed a minimum at flameout. During the afterglow, all flame retarded rubbers except R-2 worked as afterglow suppressors, reducing the COP. Because TOF was almost completely decomposed during the burning phase and did not form additional char, the remaining residue was less protected, and showed even higher COP values than the unfilled rubber R. In general, the flame retarded rubbers containing only APP and no TOF showed lower values for COP. The reduction in COP in all flame retarded rubbers resulted from increased thermal stability of the top layer of the residue.

A single parameter from the cone calorimeter measurements cannot describe the real flame spread above the surface of the specimen without oversimplifying the scenario [57]. To overcome this issue two values are widely used; the fire growth rate (FIGRA) and the maximum average rate of heat emission (MARHE) [51, 57]. The FIGRA and MARHE values are listed in Table 8. The unfilled rubber R showed a FIGRA value of 7.1 kW m^{-2} s^{-1} and an MARHE value of 314 kW m^{-2}. Table 8 showed that APP in R-1 reduced FIGRA and MARHE sufficiently, because of increased residue, as well as thermally stable char and increased gas phase activity compared to R. In contrast, the TOF in R-2 left FIGRA unchanged and resulted in a 10% increase in MARHE, because of less residue formation and lower gas phase activity than in the unprotected rubber R. Furthermore, the poor performance of R-2 resulted from the softening effect of TOF. Softer rubbers burn more easily than hard rubbers. The combination R-1/2 showed FIGRA values like R and a small reduction in MARHE, as APP partly compensated the negative impact of TOF. The addition of PANI had no effect on FIGRA or MARHE. High amounts of ATH led to a 45% reduction in FIGRA to 3.9 kW m^{-2} s^{-1} and 55% in MARHE to 142 kW m^{-2}. In general, APP and ATH formed more stable residue, which limited the flame spread.

CONCLUSIONS

In this study, eight EPDM rubbers with systematically varied content of the flame retardants APP, TOF, PANI, and ATH were prepared and investigated. The homogenous dispersion of the fillers in the rubber matrix was confirmed by the SEM mircrographs. The rheological measurements showed that the phosphorous flame retardants APP and TOF experienced plasticizing effects. These effects were compensated by the fillers PANI and ATH. As a result, the multicomponent rubber composites R-1AP and R-1/2AP preserved the vulcanization properties, while simultaneously allowing high loadings of flame retardants. The DMA revealed that the addition of TOF enabled the variation of the glass transition temperature. Furthermore, the rubbers R-1, R-1P, R-1AP, and R-1/2AP experienced improved elongation at break and Young's modulus, and showed no deterioration of the mechanical properties. In the TGA, the determined residues of the EPDM compounds were in good accordance with the calculated residue. Therefore, no additional char was formed, and no interplay of the flame retardants was detected. The Py-GC/MS investigated the pyrolysis products of the EPDM rubbers, identifying 27 compounds. The Py-GC/MS pyrograms revealed a greater number of pyrolysis products for the flame retarded rubber compounds, but indicated no interplay of the flame retardants during the pyrolysis. In the fire tests, the EPDM compounds R-1, R-1P, R-1AP, and R-1/2AP performed best in terms of LOI, UL 94, and glow wire test, and experienced self-extinguishment in FMVSS 302. In the cone calorimeter test the EPDM rubbers R-1AP and

R-1/2P achieved an increase in residue of 76% and a reduction in THE of about 35%. Furthermore, the compounds R-1AP and R-1/2P achieved a reduction in MAHRE to about 150 kW m^{-1}, an improvement of over 50% compared to the unprotected rubber R.

ACKNOWLEDGMENTS

The authors thank B. Kraft and F. Engelmann for the preparation of the EPDM rubbers, M. Morys and M. Günther for the SEM micrographs, C. Huth for the dynamic mechanical measurements, Nabaltec AG, Rheinchemie and Clariant for supporting us with materials. This research did not receive any specific grant from funding agencies in the public, commercial, or not-for-profit sectors.

CONFLICT OF INTEREST

The authors declare no conflict of interest.

REFERENCES

1. Y.Y. Yen, H.T. Wang, and W.J. Guo, *J. Appl. Polym. Sci.*, **130**, 2042 (2013). https://doi.org/10.1002/app.39394.
2. A. Kremers, A. Krusche, and E. Haberstroh, *Macromol. Mater. Eng.*, **284–285**, 70 (2000). https://doi.org/10.1002/1439-2054(20001201)284:1<70::AID-MAME70>3.0.CO;2-Y.
3. L. Ibarra, P. Posadas, and M. Esteban-Martínez, *J. Appl. Polym. Sci.*, **97**, 1825 (2005). https://doi.org/10.1002/app.21954.
4. E.D.L. Weil and S.V. Levchik, "Flame Retardants for Plastics and Textiles," in *Practical Application*. 2nd ed., Carl Hansen Verlag, Munich, Germany (2015).
5. S.V. Levchik, *J. Fire Sci.*, **24**, 345 (2006). https://doi.org/10.1177/0734904106068426.
6. D.J. Kind and T.R. Hull, *Polym. Degrad. Stab.*, **97**, 201 (2012). https://doi.org/10.1016/j.polymdegradstab.2011.12.008.
7. W.E. Horn, "Inorganic Hydroxides and Hydroxycarbonates: Their Function and Use as Flame-Retardant Additives," in *Fire Retardandancy of Polymeric Materials*, W.E. Horn, Ed., Dekker, New York, 285 (2000).
8. P.R. Hornsby, *Macromol. Symp.*, **108**, 203 (1996). https://doi.org/10.1002/masy.19961080117.
9. B. Zirnstein, W. Tabaka, D. Frasca, D. Schulze, and B. Schartel, *Polym. Test.*, **66**, 268 (2018). https://doi.org/10.1016/j.polymertesting.2018.01.035.
10. P.R. Hornsby, *Int. Mater. Rev.*, **46**, 199 (2001). https://doi.org/10.1179/095066001771048763.
11. C. Wang, L. Hong, and C. Tian, *Polym. Eng. Sci.*, **59**, 2136 (2019). https://doi.org/10.1002/pen.25216.
12. S. Yang, Y. Hu, and Q. Zhang, *High Perform. Polym.*, **31**, 186 (2019). https://doi.org/10.1177/0954008318756496.
13. S. Yang, J. Wang, S. Huo, M. Wang, and L. Cheng, *Ind. Eng. Chem. Res.*, **54**, 7777 (2015). https://doi.org/10.1021/acs.iecr.5b02026.
14. A. Wilke, K. Langfeld, B. Ulmer, V. Andrievici, A. Hörold, P. Limbach, M. Bastian, and B. Schartel, *Ind. Eng. Chem. Res.*, **56**, 8251 (2017). https://doi.org/10.1021/acs.iecr.7b01177.
15. P. Khalili, K.Y. Tshai, D. Hui, and I. Kong, *Compos. Part B*, **114**, 101 (2017). https://doi.org/https://doi.org/10.1016/j.compositesb.2017.01.049.
16. L. Li, Y. Qian, and C. Jiao, *Polym. Eng. Sci.*, **54**, 766 (2014). https://doi.org/10.1002/pen.23619.
17. M.-C. Despinasse and B. Schartel, *Thermochim. Acta*, **563**, 51 (2013). https://doi.org/https://doi.org/10.1016/j.tca.2013.04.006.
18. S. Yang, J. Wang, S. Huo, M. Wang, J. Wang, and B. Zhang, *Polym. Degrad. Stab.*, **128**, 89 (2016). https://doi.org/https://doi.org/10.1016/j.polymdegradstab.2016.03.017.
19. U. Braun, H. Bahr, H. Sturm, and B. Schartel, *Polym. Adv. Technol.*, **19**, 680 (2008). https://doi.org/10.1002/pat.1147.
20. B. Schartel and G. Schmaucks, *Polym. Eng. Sci.*, **57**, 1099 (2017). https://doi.org/10.1002/pen.24485.
21. F. Lou, K. Wu, Q. Wang, Z. Qian, S. Li, and W. Guo, *Polymers*, **11**, 125 (2019). https://doi.org/.
22. U. Braun and B. Schartel, *Macromol. Chem. Phys.*, **205**, 2185 (2004). https://doi.org/10.1002/macp.200400255.
23. K.H. Pawlowski and B. Schartel, *Polym. Degrad. Stab.*, **93**, 657 (2008). https://doi.org/https://doi.org/10.1016/j.polymdegradstab.2008.01.002.
24. E. Wawrzyn, B. Schartel, A. Karrasch, and C. Jäger, *Polym. Degrad. Stab.*, **106**, 74 (2014). https://doi.org/https://doi.org/10.1016/j.polymdegradstab.2013.08.006.
25. J. Reuter, L. Greiner, F. Schönberger, and M. Döring, *J. Appl. Polym. Sci.*, **136**, 47270 (2019). https://doi.org/10.1002/app.47270.
26. T.D. Hapuarachchi and T. Peijs, *Express Polym. Lett.*, **3**, 743 (2009). https://doi.org/10.3144/expresspolymlett.2009.92.
27. B. Zirnstein, D. Schulze, and B. Schartel, *Materials*, **12**, 1932 (2019). https://doi.org/10.3390/ma12121932.
28. A. Castrovinci, G. Camino, C. Drevelle, S. Duquesne, C. Magniez, and M. Vouters, *Eur. Polym. J.*, **41**, 2023 (2005). https://doi.org/https://doi.org/10.1016/j.eurpolymj.2005.03.010.
29. S. Moon, B. Jo, and R.J. Farris, *Polym. Compos.*, **30**, 1732 (2009). https://doi.org/doi:10.1002/pc.20794.
30. H. Wang and J. Tian, *J. Wuhan Univ. Technol.-Mater. Sci. Ed.*, **28**, 706 (2013). https://doi.org/10.1007/s11595-013-0756-8.
31. Z. Wang, X. Zhang, C. Bao, Q. Wang, Y. Qin, and X. Tian, *J. Appl. Polym. Sci.*, **124**, 3487 (2012). https://doi.org/10.1002/app.35460.
32. B. Zirnstein, D. Schulze, and B. Schartel, *Thermochim. Acta*, **673**, 92 (2019). https://doi.org/10.1016/j.tca.2019.01.019.
33. *Reaction-to-Fire Tests—Heat Release, Smoke Production and Mass Loss Rate—Part 1: Heat Release Rate (Cone Calorimeter Method) and Smoke Production Rate (Dynamic Measurement)*, ISO, Geneva, Switzerland (2015). https://doi.org/.
34. B. Schartel, M. Bartholmai, and U. Knoll, *Polym. Degrad. Stab.*, **88**, 540 (2005). https://doi.org/10.1016/j.polymdegradstab.2004.12.016.
35. A.R. Horrocks, G. Smart, S. Hörold, W. Wanzke, E. Schlosser, and J. Williams, *Polym. Degrad. Stab.*, **104**, 95 (2014). https://doi.org/10.1016/j.polymdegradstab.2014.03.027.
36. N. Wang, L. Mi, Y. Wu, J. Zhang, and Q. Fang, *J. Therm. Anal. Calorim.*, **115**, 1173 (2013). https://doi.org/10.1007/s10973-013-3404-9.
37. G. Oenslager, *Ind. Eng. Chem.*, **25**, 232 (1933). https://doi.org/10.1021/ie50278a031.
38. A.Y. Coran, *Rubber Chem. Technol.*, **68**, 351 (1995). https://doi.org/10.5254/1.3538748.
39. A. Malas, P. Pal, and C.K. Das, *Mater. Des.*, **55**, 664 (2014). https://doi.org/10.1016/j.matdes.2013.10.038.

40. J. Oh, Y.H. Yoo, I.-S. Yoo, Y.-I. Huh, T.K. Chaki, and C. Nah, *J. Appl. Polym. Sci.*, **131**, 39795 (2014). https://doi.org/10.1002/app.39795.
41. P.L. Teh, Z.A. Mohd Ishak, A.S. Hashim, J. Karger-Kocsis, and U.S. Ishiaku, *Eur. Polym. J.*, **40**, 2513 (2004). https://doi.org/10.1016/j.eurpolymj.2004.06.025.
42. S. Ansorge and K. Papailiou, *J. Elastom. Plast.*, **48**, 354 (2015). https://doi.org/10.1177/0095244315580452.
43. P. Salvatore, *Intumescent Flame Retarded Polypropylene Systems Containing Sepiolite Clays: Properties and Synergic Effects*, Università degli Studi di Napoli Federico II, Naples, Italy (2016).
44. R. Faez and M.-A. De Paoli, *Eur. Polym. J.*, **37**, 1139 (2001). https://doi.org/https://doi.org/10.1016/S0014-3057(00)00235-4.
45. X.L. He, W.H. Guo, and C.F. Wu, *J. Plast. Rubber Compos.*, **36**, 149 (2007). https://doi.org/10.1179/174328907X191422.
46. M.A. Soto-Oviedo, O.A. Araújo, R. Faez, M.C. Rezende, and M.-A. De Paoli, *Synth. Met.*, **156**, 1249 (2006). https://doi.org/10.1016/j.synthmet.2006.09.003.
47. S.-S. Choi and Y.-K. Kim, *Polym. Test.*, **30**, 509 (2011). https://doi.org/10.1016/j.polymertesting.2011.04.005.
48. A.B. Nair, U.G. Kalappura, P. Kurian, and R. Joseph, *Polym. Eng. Sci.*, **53**, 699 (2013). https://doi.org/10.1002/pen.23314.
49. E.D.W. Menachem Lewin, *Fire Retardant Materials*, Vol. **1**, Woodhead Publishing Limited, Cambridge, England (2001).
50. B. Schartel, *Materials*, **3**, 4710 (2010). https://doi.org/10.3390/ma3104710.
51. B. Schartel and T.R. Hull, *Fire Mater.*, **31**, 327 (2007). https://doi.org/10.1002/fam.949.
52. S. Brehme, B. Schartel, J. Goebbels, O. Fischer, D. Pospiech, Y. Bykov, and M. Döring, *Polym. Degrad. Stab.*, **96**, 875 (2011). https://doi.org/10.1016/j.polymdegradstab.2011.01.035.
53. B. Schartel, B. Perret, B. Dittrich, M. Ciesielski, J. Krämer, P. Müller, V. Altstädt, L. Zang, and M. Döring, *Macromol. Mater. Eng.*, **301**, 9 (2016). https://doi.org/10.1002/mame.201500250.
54. M. Sahnoune, A. Taguet, B. Otazaghine, M. Kaci, and J.-M. Lopez-Cuesta, *Polym. Eng. Sci.*, **59**, 526 (2019). https://doi.org/10.1002/pen.24961.
55. B. Schartel, M. Bartholmai, and U. Knoll, *Polym. Adv. Technol.*, **17**, 772 (2006). https://doi.org/10.1002/pat.792.
56. A. Sut, S. Greiser, C. Jäger, and B. Schartel, *Thermochim. Acta*, **640**, 74 (2016). https://doi.org/10.1016/j.tca.2016.08.004.
57. E. Gallo, B. Schartel, G. Schmaucks, K. von der Ehe, and M. Bohning, *Plast. Rubber Compos.*, **42**, 34 (2013). https://doi.org/10.1179/1743289812y.0000000012.